REPORT DOCUMENTATION PAGE

Form Approved
OMB No. 0704-0188

PLEASE DO NOT RETURN YOUR FORM TO THE ABOVE ADDRESS.

1. REPORT DATE *(DD-MM-YYYY)*	2. REPORT TYPE	3. DATES COVERED *(From - To)*
March 1, 2007	Final Report	7/1/2002-12/31/2006

4. TITLE AND SUBTITLE

Designing of Bulk Nano-structures with Enhanced Thermoelectric Properties

5a. CONTRACT NUMBER

5b. GRANT NUMBER

N00014-02-1-0867

5c. PROGRAM ELEMENT NUMBER

6. AUTHOR(S)

Mercouri G Kanatzidis
Department of Chemistry
Michigan State University
East Lansing, MI 48824

5d. PROJECT NUMBER

NA

5e. TASK NUMBER

NA

5f. WORK UNIT NUMBER

NA

7. PERFORMING ORGANIZATION NAME(S) AND ADDRESS(ES)

Michigan State University
East Lansing, MI 48824

8. PERFORMING ORGANIZATION REPORT NUMBER

4

9. SPONSORING/MONITORING AGENCY NAME(S) AND ADDRESS(ES)

Office of Naval Research
875 Randolph St
One Liberty Center
Arlington, VA 22203-1995

10. SPONSOR/MONITOR'S ACRONYM(S)

ONR

11. SPONSOR/MONITOR'S REPORT NUMBER(S)

NA

12. DISTRIBUTION/AVAILABILITY STATEMENT

Approved for public release. Distribution is unlimited

13. SUPPLEMENTARY NOTES

NA

14. ABSTRACT

We discovered a grand homologous series which may help in the future to systematically identify thermoelectric materials with high performance. Namely, the series Am[M1+lSe2+l]2m[M2l+nSe2+3l+n] (A = alkali metal, M = Pb, Bi) has structure-predicting properties. The modular construction of these structures from evolving building blocks permits many of the criteria necessary for good thermoelectrics to be met. K2Bi8Se13 is a member of this series and was found to be a promising thermoelectric. The charge transport properties were studied under pressure, where a significant increase in the power factor was observed. Several other promising materials were also discovered. In another part of this project we prepared nanocrystals of thermoelectric semiconductors and studied their properties. We investigated the assembly of nanocrystal components into well-organized arrays. The goal was to utilize quantum dot building blocks of desired thermal and electronic properties to design composite materials with improved power generation, thermoelectric characteristics. We devised new ways to prepare nanocrystals of PbTe, AgSbTe2 and AgPb2SbTe4.

15. SUBJECT TERMS

Thermoelectric materials, semiconductors, nanocrystals, quantum dots

16. SECURITY CLASSIFICATION OF:			17. LIMITATION OF ABSTRACT	18. NUMBER OF PAGES	19a. NAME OF RESPONSIBLE PERSON
a. REPORT	b. ABSTRACT	c. THIS PAGE			Mercouri G Kanatzidis
U	U	U	UU	19	19b. TELEPHONE NUMBER *(Include area code)* 847-467-1541

ONR (N00014-02-1-0867)

Designing of Bulk Nano-structures with Enhanced Thermoelectric Properties

ONR Program Manager:
Dr Mihal Gross

Professor MERCOURI KANATZIDIS
Professor TIMOTHY HOGAN
(with Dr Chris Murray IBM)

Michigan State University
East Lansing, MI 48824

Project ending date:
12/31/2006

FINAL REPORT
April 23, 2007

ONR (N00014-02-1-0867)
MERCOURI KANATZIDIS, TIM HOGAN, (with Chris Murray IBM)
FINAL REPORT
April 23, 2007

Designing of Bulk Nano-structures with Enhanced Thermoelectric Properties

Phase 1: New thermoelectric materials through phase homologies

Part of this project involved the synthesis and investigation of novel ternary chalcogenide materials for thermoelectric applications. The $K_2Bi_8Se_{13}$ material was extensively investigated. It was found that it has a very low thermal conductivity and highly anisotropic charge transport and thermal transport properties. Charge transport and thermal conductivity measurements on doped $K_2Bi_8Se_{13}$ showed a thermal conductivity of ~1.3 W/m·K and relatively high power factor ($S^2 \cdot \sigma$ ~12 μW/cm·K^2). The Seebeck coefficient is negative indicating n-type character while its temperature dependence as well as that of electrical conductivity suggests a highly degenerate semiconductor. The charge transport properties have also been studied under pressure, where a significant increase in the power factor as well as a peak in the Seebeck coefficient was observed, suggesting electronic topological transition upon compression.

The charge transport properties of the low-dimensional thermoelectric materials $K_2Bi_{8-x}Sb_xSe_{13}$ ($0<x\leq 8$) were studied as a function of temperature and composition. The Seebeck coefficient shows an evolution from n-type to p-type character with increasing incorporation of Sb and at the same time the temperature dependence of the electrical conductivity changes from that of a degenerate semiconductor to that of an intrinsic or compensated semiconductor. These changes however are not monotonic with composition due to the non-uniform substitution of Sb atoms at the Bi sites of the structure. Three separate composition regions can be assigned depending on x each with different charge transport character. Electronic transport in $K_2Bi_{8-x}Sb_xSe_{13}$ was analyzed on the basis of classical semiconductor theory and discussed in the context of recent band calculations. The results suggest that the $K_2Bi_{8-x}Sb_xSe_{13}$ materials possess coexisting domains with semimetallic and semiconducting character whose ratio is influenced by the value of x and by local defects. The extent and relative distribution of these domains control the charge transport properties. Electron diffraction experiments performed on samples of $K_2Bi_{8-x}Sb_xSe_{13}$ with x=1.6 show evidence for such domains by indicating regions with long range ordering of K^+/Bi^{3+} atoms and regions with increased disorder. The semiconducting behavior is enhanced with increasing x (i.e. Sb/Bi ratio) in the composition through a decrease of the semimetallic fraction.

Physical insights concerning structure-property relationships in the $K_2Bi_{8-x}Sb_xSe_{13}$ series were obtained from studies of charge transport properties. Increasing incorporation of Sb in $K_2Bi_8Se_{13}$ leads to an enhancement of the semiconducting character and a gradual conversion from n- to p-type transport. The property evolution is not monotonic with composition due to the non-uniform Bi/Sb/K substitution and distribution. The transport in these materials particularly for $x<5.6$ can be understood in the context of coexisting semimetallic and semiconducting domains in the crystal. On the Bi-rich side, a finite-gap semiconductor model, with the addition of a significant concentration of shallow donors (N_0), which remain ionized even at low temperatures accounts for the free carrier behavior. The origin of the N_0 donors seems to be associated with degree of order / or disorder at the mixed occupancy M/K sites. The co-existence of M/K disorder and long range ordering on the M/K sites which was shown by electron diffraction is responsible for the observed charge transport properties of these materials. Therefore careful control of the growth conditions may reduce the semimetallic contributions and permit a significant enhancement of the thermoelectric properties through the change of the degree of disorder at the K/M sites.
When the content of Sb increases toward the Sb-rich end of the series, the disorder is reduced and finally eliminated in end compound $K_2Sb_8Se_{13}$. Beyond the normal increase of band gap with Sb incorporation,

the gradual elimination of the disorder reveals a progressively more semiconducting character of $K_2Bi_{8-x}Sb_xSe_{13}$. As the N_0 source of free electrons is depleted, the p-character is strongly enhanced. The n- to p-type evolution with rising Sb fraction in the series $K_2Bi_{8-x}Sb_xSe_{13}$ seems to occur at the boundary of compositional region B and C. This seems to be a critical compositional region in which the system changes transport behavior and is of great interest for future studies. It needs to be further investigated by studying compounds with $x \sim 5.5$. We found that materials in this region exhibit enormous thermopower and have the potential to produce a high power factor ($\sigma \cdot S^2$) at high temperature.

Homologous Series

We discovered a grand homologous series which may help in the future to systematically identify thermoelectric materials with high performance. Namely, the series $A_m[M_{1+l}Se_{2+l}]_{2m}[M_{2l+n}Se_{2+3l+n}]$ (A = alkali metal, M = Sn, Pb, Sb, Bi) have composition and structure-predicting properties. The modular construction of these structures from evolving building blocks (nanorods and layers) permits many of the criteria necessary for good thermoelectrics to be met. These include very anisotropic effective mass ratio, appropriate energy gap and exceedingly low thermal conductivity. We described these homologous series in a review article in *Account of Chemical Research.*

(a) One-dimensional structures. The homologous superseries $A_m[M_{1+l}Se_{2+l}]_{2m}[M_{2l+n}Se_{2+3l+n}]$ can derive a large number of compounds prepared by controlling the three variable integers *l*, *m* and *n*. The construction of each member is modular and phase assembly is achieved by two different modules, $[M_{2l+n}Se_{2+3l+n}]$ and $[M_{1+l}Se_{2+l}]_{2m}$ of adjustable dimensions. The modules are linked to a three-dimensional framework with tunnels that accommodate the alkali ions (A_m). The $[M_{1+l}Se_{2+l}]_{2m}$ and $[M_{2l+n}Se_{2+3l+n}]$ modules represent various fragments from the NaCl lattice sliced along different orientation and dimensions. Usually they vary in dimension along two directions of the NaCl lattice while the third dimension is infinite. $[M_{1+l}Se_{2+l}]_{2m}$ represents the $NaCl^{100}$ type module and $[M_{2l+n}Se_{2+3l+n}]$ represents the $NaCl^{111}$-type module. The manner in which these modules connect gives rise to strongly anisotropic structures. The size and shape of these building blocks is *adjustable*. While the thickness of the $NaCl^{100}$ type units is given by *m*, the shape of the $NaCl^{111}$ type units is controlled by *n*. The integer *l* sets the width, i.e. the number of MSe_6 octahedra, of *both* modules.

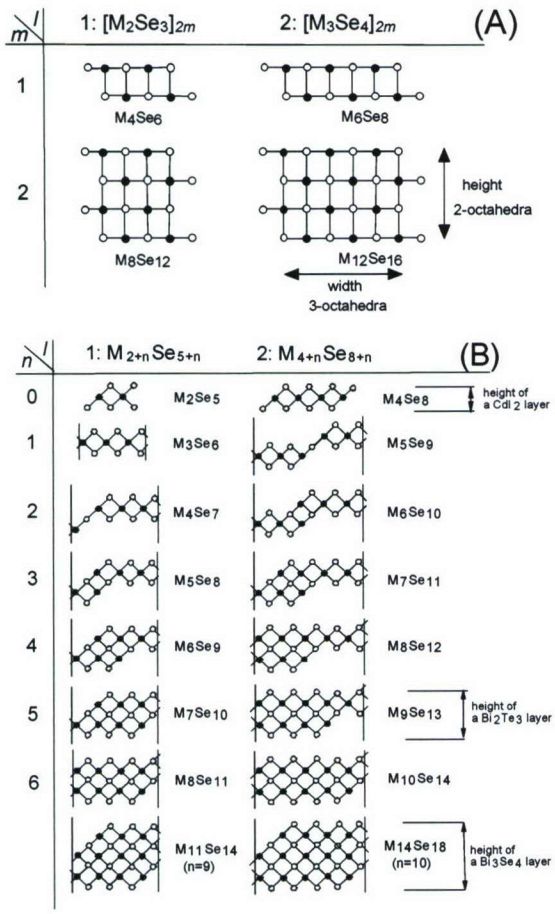

Figure 1. (A) Structure of $NaCl^{100}$ type modules for various *l* and *m* values. The height and width are a few nm and are indicated. (B) $NaCl^{100}$ type modules for various *l* and *m* values.

Figure 1 illustrates the structures of the two types of modules and how they evolve systematically with the variables *l*, *m* and *n*. Every member of the series represents a different structure type. Clearly, these materials possess fragments of nanosized dimensions, and so even though this class of materials consists of pure single-phase compounds, they have clearly recognizable nanostructural characteristics. These moieties, as

they evolve from one member to the next, systematically influence the charge and thermal transport properties. For example, the structural modules that make up the structure of $K_2Bi_8Se_{13}$ (Figure 2) lead to an anisotropic effective mass ratio and exceedingly low thermal conductivity, important criteria for thermoelectric performance.

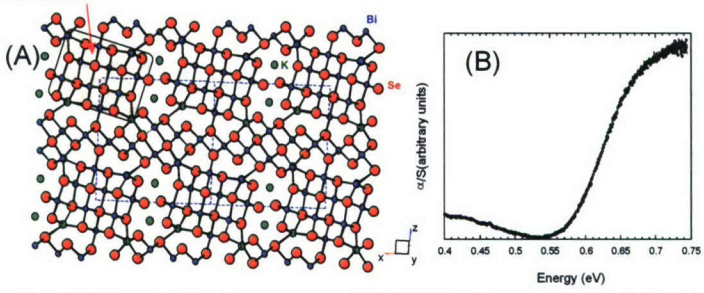

Figure 2. (A) Example of a highly anisotropic compound ($K_2Bi_8Se_{13}$) composed of linked infinite nano-sized rods (shaded area) and layers. The nanorods have rectangular cross section and are separated with weakly interacting K ions. (B) Infrared absorption spectrum of $K_2Bi_8Se_{13}$ showing a band gap of 0.58 eV.

In general, modifying the three integers *l*, *m* and *n* provides three different ways to change *predictably* the structure of known compounds. The structure types possible for $l = 2$ with $m = 1$ and 2 are depicted in Figure 3, which illustrates how higher members evolve from lower ones by adding MSe equivalents to the initial NaCl[111] type layers. The absence of members with $n = 1, 3$ etc means these members have not yet been observed, but they are predicted to exist and can for example be future synthetic targets.

In $K_2Bi_8Se_{13}$ (a member of the homology) we clearly demonstrated very low lattice thermal conductivity of 0.8 W/m·K. Its energy gap is a desirable 0.58 eV, Figure 2b. $K_2Bi_8Se_{13}$ samples doped with Sn show promising results. For example, single crystals of 0.5% Sn-doped $K_2Bi_8Se_{13}$, gave a maximum power factor of 38 $\mu W/cm \cdot K^2$ at 295 K. This value is ~ 3-fold higher than that of undoped $K_2Bi_8Se_{13}$. With a typical thermal conductivity of ~1.4 W/m·K, the ZT of this sample reaches ~0.9 at room temperature, with the trend pointing even higher at high temperatures, reaching values of 1.4 to 1.7. Data obtained at JPL (T. Caillat) on cold-pressed polycrystalline (randomly oriented) samples show ZT of 1 at 650 K, even with a very low electrical conductivity of 90 S/cm! We expect the thermopower to maximize at >700 K between 350-450 μV/K. Using highly oriented ingot samples (0.5% Pb doped) we have measured room temperature electrical conductivity and thermopower of ~1120 S/cm and –110 μV/K, respectively. The thermopower rises to -280 μV/K at 700 K. This is an exciting finding and highlights the potential of the homologous series to produce promising candidates.

Another member, $KPb_4Bi_7Se_{15}$, is also promising as our data indicates. Polycrystalline samples show a room temperature electrical conductivity of 550 S/cm and a large negative Seebeck coefficient, -150 μV/K, at room temperature. The Seebeck coefficient continues to rise up to the highest temperature measured of 700 K and reaches a value of -280 μV/K, Figure 4. The thermal conductivity, κ_{meas}, measured along the needle axis of an oriented ingot shows a room temperature value of only ~0.65 W/m·K, see Figure 15. We expect that high quality ingots grown from this system should exhibit high carrier mobilities and a large ZT at ~700-800 K. $KPb_9Bi_{11}Se_{26}$ exhibits similarly promising behavior with a moderately high room temperature electrical conductivity (570 S/cm) and Seebeck coefficient (-110 μV/K). At 600 K the thermopower is -230 μV/K. The compound is a narrow gap semiconductor with a band gap of ~ 0.50 eV.

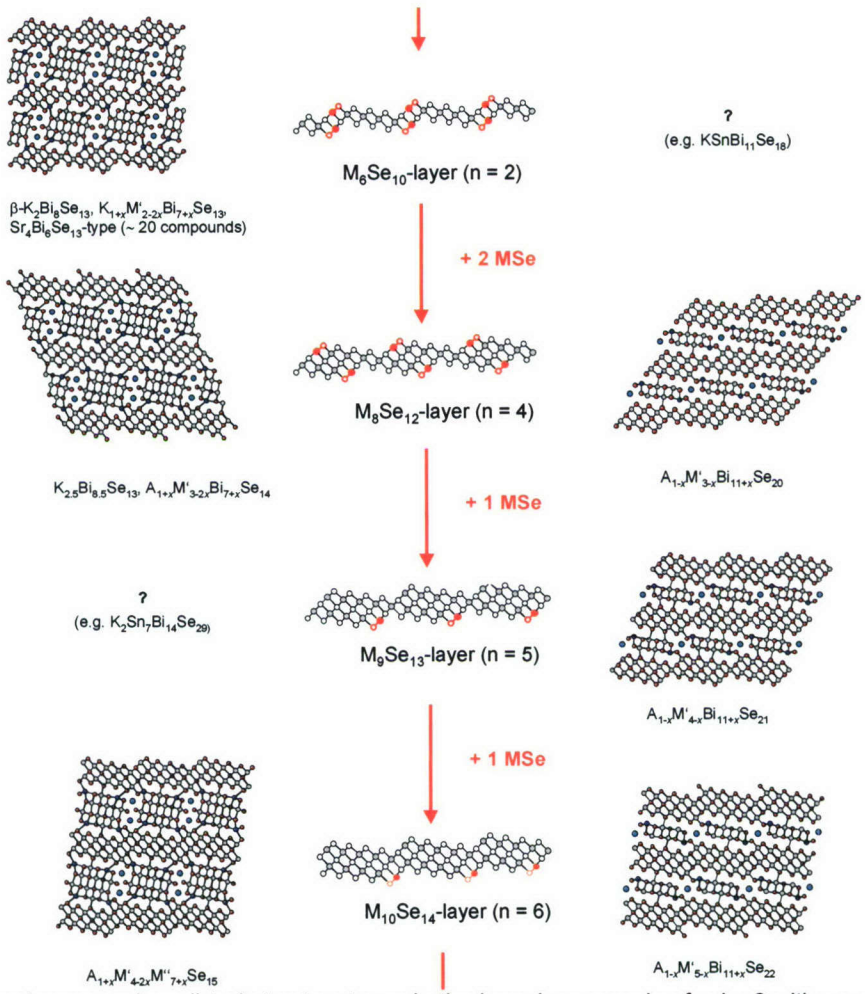

Figure 3. Various known and predicted structure types in the homologous series for $l = 2$ with $m = 1$ and 2. Places with question marks indicate predicted phases.

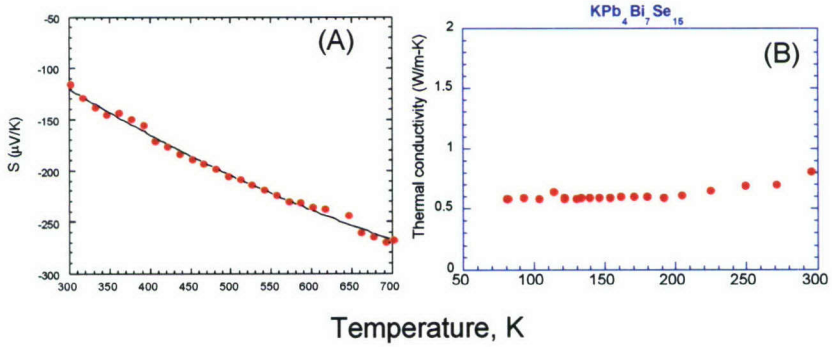

Figure 4. (left) High temperature Seebeck coefficient for $KPb_4Bi_7Se_{15}$. (right) Extremely low thermal conductivity κ_{meas} of $KPb_4Bi_7Se_{15}$.

Crystal Growth, Thermoelectric Properties and Electronic Structure of $AgBi_3S_5$ and $AgSb_xBi_{3-x}S_5$ (x=0.3)

We prepared and studied synthetic pavonite, $AgBi_3S_5$, and its derivative $AgSb_xBi_{3-x}S_5$ (x = 0.3) and evaluated their potential as thermoelectric materials. The crystal structure refinements, crystal growth, physico-chemical properties, band structure calculations and exceptionally low thermal conductivity of these materials were also studied.

$AgBi_3S_5$ and $AgSb_xBi_{3-x}S_5$ were synthesized by reacting the elemental mixtures (Ag:Bi:S = 1:3:5.25, Ag:Sb:Bi:S = 1:x:3-x:5.25) in a torch flame. A slight excess of S was added to compensate a loss of sulfur vaporized from the top surface of the molten mixture during the reaction. The $AgSb_xBi_{3-x}S_5$ series of compounds with several x values (up to x = 1) were investigated. The $AgSb_xBi_{3-x}S_5$ with x = 0.1, 0.2, 0.3, and 0.5 produced pure solid solutions, while the x = 1 provided a mixture of the $AgSb_xBi_{3-x}S_5$ solid solution and Bi_2S_3. This is not surprising since $AgSb_3S_5$ (i.e. x = 3) is not a stable compound. $AgBi_3S_5$ and $AgSb_{0.3}Bi_{2.7}S_5$ appear to melt congruently at 735 and 723 °C, respectively. For both compounds a comparison of the X-ray powder diffraction patterns before and after the DTA experiments showed no significant phase change.

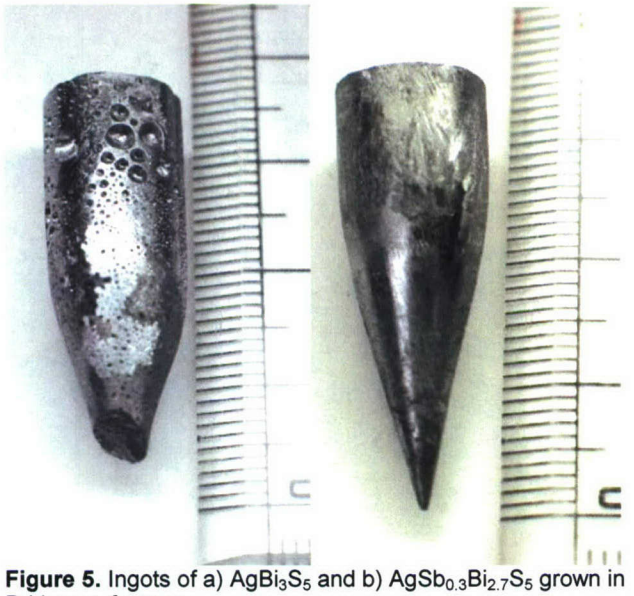

Figure 5. Ingots of a) $AgBi_3S_5$ and b) $AgSb_{0.3}Bi_{2.7}S_5$ grown in Bridgman furnace.

For thermal and electrical conductivity measurements we grew large crystals of $AgBi_3S_5$ and $AgSb_{0.3}Bi_{2.7}S_5$ using the Bridgman technique. The obtained ingots show well grown highly oriented characteristics, Figure 5. The natural crystal habit of these compounds is to grow as long planks and in the ingots the long axis (crystallographic *b*-axis) lies parallel to the Bridgman translation axis. These ingots were cut along the direction parallel and perpendicular to the crystal growth. Experimental evidence that a very high degree of crystal orientation was achieved in the ingots was obtained from X-ray diffraction data taken on cut specimens along different directions, Figure 6. The presence of a certain class of reflections when the X-ray beam is incident along one direction (e.g. (*h2l*) in Figure 6f) and their complete absence when the beam is incident along a perpendicular direction (e.g. in Figure 2d) is proof that a nearly perfect (estimated at >96%) crystallographic orientation has been achieved.

$AgBi_3S_5$ has a strongly anisotropic three-dimensional framework composed of two types of slabs which can be described as an assembly of blocks excised from the cubic NaCl structure type. These blocks are two-dimensional slabs excised by slicing perpendicular to the [311] direction of the NaCl lattice, Figure 7.

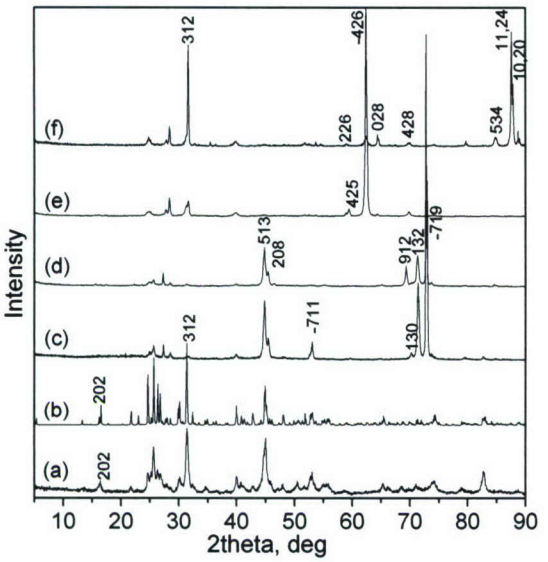

Figure 6. XRD patterns of $AgBi_3S_5$ (a) of polycrystalline powdered sample, (b) calculated from the crystal structure, (c) well grown ingot sample with an X-ray beam along *a* direction on *ab* plane, (d) *b* direction on *ab* plane, (e) *b* direction on *bc* plane and (f) *c* direction on *bc* plane.

The thinner slab (slab I) is composed of single $[AgS_6]$ octahedron sandwiched by two square pyramids of $[BiS_5]$. The thicker slab (slab II) is made of distorted galena-type structure with one $[AgS_6]$ and four $[BiS_6]$ octahedra per one diagonal octahedral chain. The two slabs are interconnected through sharing atom S(4). This modular construction gives the compound a highly anisotropic morphology and electronic structure.

All members of the solid solutions $AgSb_xBi_{3-x}S_5$ we prepared are isostructural to $AgBi_3S_5$.

Energy gaps and electronic band structure calculations. Electronic band structure calculations can be an important tool to explore the properties of materials. It not only can rationalize the observed properties but can also provide guidance for further modifications toward a desired direction. To the best of our knowledge band structure calculations on $AgBi_3S_5$ (pavonite) have not been reported. Thus we first carried out electronic band structure calculations to understand the influence of the crystal structure on the electronic structure and properties of $AgBi_3S_5$ and $AgSb_{0.3}Bi_{2.7}S_5$. We also examine how each element contributes to the conduction band and valence band structure near the Fermi energy level.

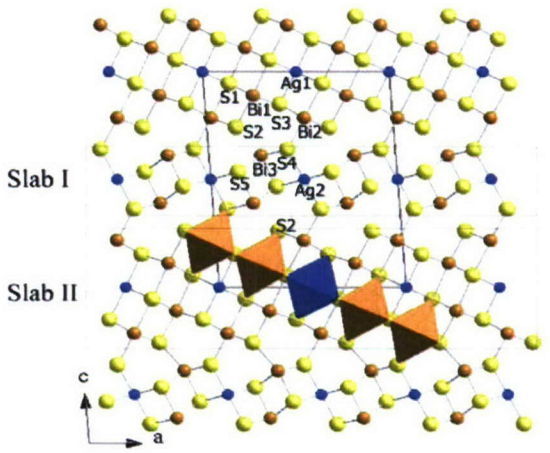

Figure 7. Projection of the structure of $AgBi_3S_5$ down the *b*-axis. Two slabs can be described by slightly distorted layers cut along the (311) face of NaCl-type structure. The slab (II) includes five octahedra per one diagonal octahedral chain. In the structure of $AgSb_{0.3}Bi_{2.7}S_5$ the Bi(1) and Bi(2) sites are disordered with Sb atoms.

Electronic structure calculations show that $AgBi_3S_5$ is an indirect narrow band-gap semiconductor with a energy gap of ~0.17 eV, Figure 8 and 9A. Density of states(DOS) analysis shows that the high valence band states in the range from -0.75 to 0 eV consist mostly of p states of S(4) and S(5) atoms which are hybridized with d states of Ag(2), Figure 6C and D. This suggests a 2-dimensional hole transport in Slab I since S(4), S(5) and Ag(2) atoms are located in it. The bottom of the conduction band consists of p states of Bi(1) and Bi(2) atoms with very small contribution from Bi(3) atoms, Figure 9B. The Bi(1) and Bi(2) p states are hybridized with the p states of S(1), S(2), and S(3) atoms in the range from 0 to 1 eV, suggesting that the electron transport is mostly confined within Slab II. Therefore, the electron and hole transports should be separated in space. From the projected density of states calculations (Fig. 9D) we find that the filled d-states of Ag(1) and Ag(2) lie surprisingly high in energy and in the same region as the S p bands. This results in a strong mixing of the Ag d states

and the S p states and leads to two a rather narrow hybridized valence band. Due to the different local environments of Ag(1) and Ag(2), the Ag(2) associated band is about 0.75 eV higher than the Ag(1) associated band. As a result the top of the valence band and hence the hole transport takes place in slab I in which the Ag(2) atom resides, Fig 7. The narrow valence band leads to a rapidly increasing density of states near the valence band maximum which suggests that if this system could be hole-doped, it could show a very large thermopower. It will be interesting to test this prediction by making hole-doped samples.

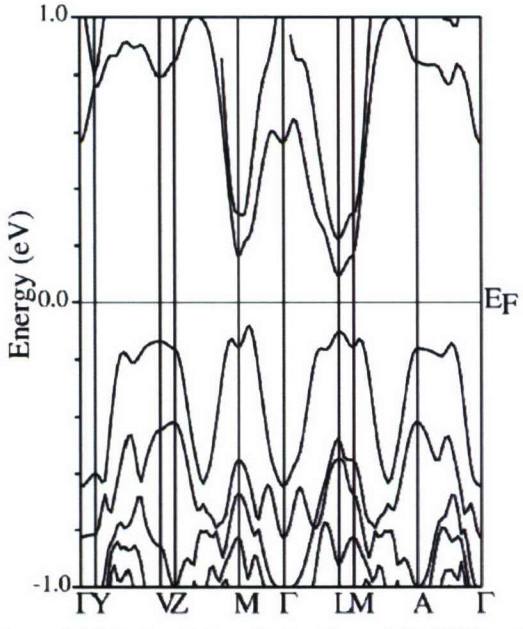

Figure 8. Electronic band structure of $AgBi_3S_5$ with spin-orbit interaction included (E_g = 0.17 eV).

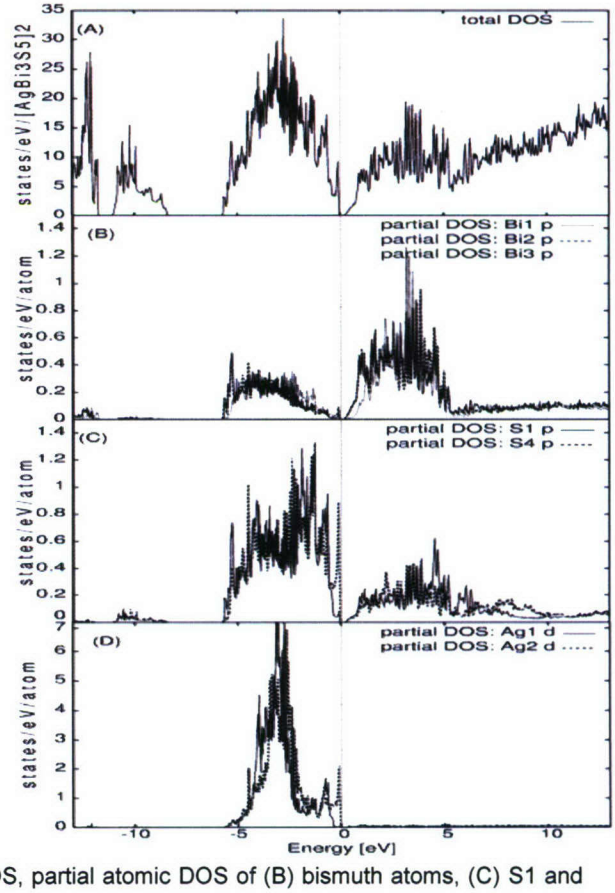

Figure 9. Density of states (DOS) of $AgBi_3S_5$. (A) Total DOS, partial atomic DOS of (B) bismuth atoms, (C) S1 and S4, and (D) silver atoms.

The optical absorption properties of $AgBi_3S_5$ and $AgSb_{0.3}Bi_{2.7}S_5$ were examined with solid state optical absorption spectroscopy. The spectra in the UV/Vis range show intense absorptions for both $AgBi_3S_5$ and $AgSb_{0.3}Bi_{2.7}S_5$ around 0.6 eV, Figure 10.

Thermoelectric properties. Thermopower measurements on samples cut from oriented polycrystalline ingots were carried out along the crystal growth direction (i.e., crystallographic *b*-axis). The thermopower of $AgBi_3S_5$ is negative and increases almost linearly from -25 μV/K at 80 K to -160 μV/K at 700 K, Figure 11(a) and 12(a). The negative value (n-type) indicates that the predominant carriers are electrons, and charge transport in this compound is accomplished by carriers moving predominantly through Bi-p orbitals near the conduction band bottom as suggested by the results of the electronic band calculations.

Electrical conductivity measurements were also performed along the direction of crystal growth. The conductivity of the $AgBi_3S_5$ ingot was relatively high and exhibited negative temperature dependence with the value decreasing almost linearly from 660 S/cm at 80 K to 134 S/cm at 700 K. This is a typical behavior for a degenerate semiconductor, Figure 11(a). It is possible that the degree of doping varies in

ingots of these materials since the electrical conductivities between two separate measurements at a low and a high temperature range showed approximately 100 S/cm gap at room temperature, Figure 11(a) and 12(a). Variations in electrical conductivities were observed in oriented ingot sample of $AgBi_3S_5$ screened by scanning probe conductivity measurements at room temperature. The scanned electrical conductivity values varied from 244 S/cm at one crystal domain to the almost twice the value with 415 S/cm at another domain which was only 0.2 mm away. Further studies regarding anisotropy of $AgBi_3S_5$ with better grown samples are planned.

Among the $AgSb_xBi_{3-x}S_5$ solid solutions the compound with x = 0.3 was selected for measuring charge transport properties. This material showed slightly lower electrical conductivity and higher thermopower than $AgBi_3S_5$ implying a lower number of carriers. The room temperature values were 260 S/cm for the conductivity and -98 μV/K for the thermopower, Figure 11(b). The thermopower of $AgSb_{0.3}Bi_{2.7}S_5$ increases almost linearly from -35 μV/K at 80 K to -150 μV/K at 400 K and the conductivity decreases from 344 S/cm at 80 K to ~200 S/cm at 400 K.

The thermal conductivity of $AgBi_3S_5$ was observed at ~1.5 W/m·K at room temperature and it increases as temperature rises from 80 K to 300 K, Figure 8(a). The thermal conductivity can be divided into two contributions, electronic κ_{ele} and lattice κ_{latt}. Because the room temperature electronic conductivity is <300 S/cm the electronic contribution is only a small fraction of the total and the lattice thermal conductivity dominates heat transport in these materials. The rising thermal conductivity with rising temperature observed in the data is due to irradiative losses (which begin to appear around 200 K) inherent in the measurement. The thermal conductivity of $AgSb_{0.3}Bi_{2.7}S_5$ showed a similarly low value (~1.6 W/m·K) at room temperature to that of $AgBi_3S_5$, Figure 11(b). Again it irradiative losses are evident in the measurement which raise the thermal conductivity.

The true value of thermal conductivity was obtained (on $AgSb_{0.3}Bi_{2.7}S_5$) using with a different method (i.e. thermal diffusivity technique) that is not subject to irradiative losses. These measurements actually showed a very low thermal conductivity of less than 1 W/m·K at the temperature, Figure 12(b). In comparison with the room temperature values obtained with the steady state technique (Figure 11(b)), the observed difference of ~0.76 W/m·K is attributed irradiative losses. At 800 K an exceptionally low value of 0.75 W/m·K is attained, Figure 12(b). These values are consistent with the low crystal symmetry, complexity of the crystal structure and the presence of heavy atoms (e.g., Bi) in the structure.

The fact that the lattice thermal conductivities of $AgBi_3S_5$ and $AgSb_{0.3}Bi_{2.7}S_5$ are similar indicates a 10% participation of Sb atoms in the Bi atom sites of solid solution is not enough to cause a significant reduction in the lattice thermal conductivity in this system.

This study emphasizes the importance of crystal growth of $AgBi_3S_5$. The calculations suggest that the silver d-states are involved near the Fermi level and influence the charge transport properties in this material. They also suggest a high thermopower in this system should p-type doping be achievable. The controlled substitution with other elements in the slabs consisting of $AgBi_3S_5$ and modification of the structure by partially replacing Ag with alkali metal, copper, or thallium could help to further modulate the thermoelectric properties in this class of compounds.

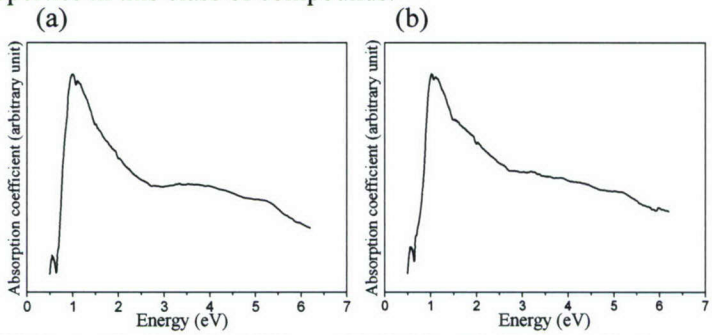

Figure 10. Solid-state UV/Vis spectra for (a) $AgBi_3S_5$ and (b) $AgSb_{0.3}Bi_{2.7}S_5$ respectively.

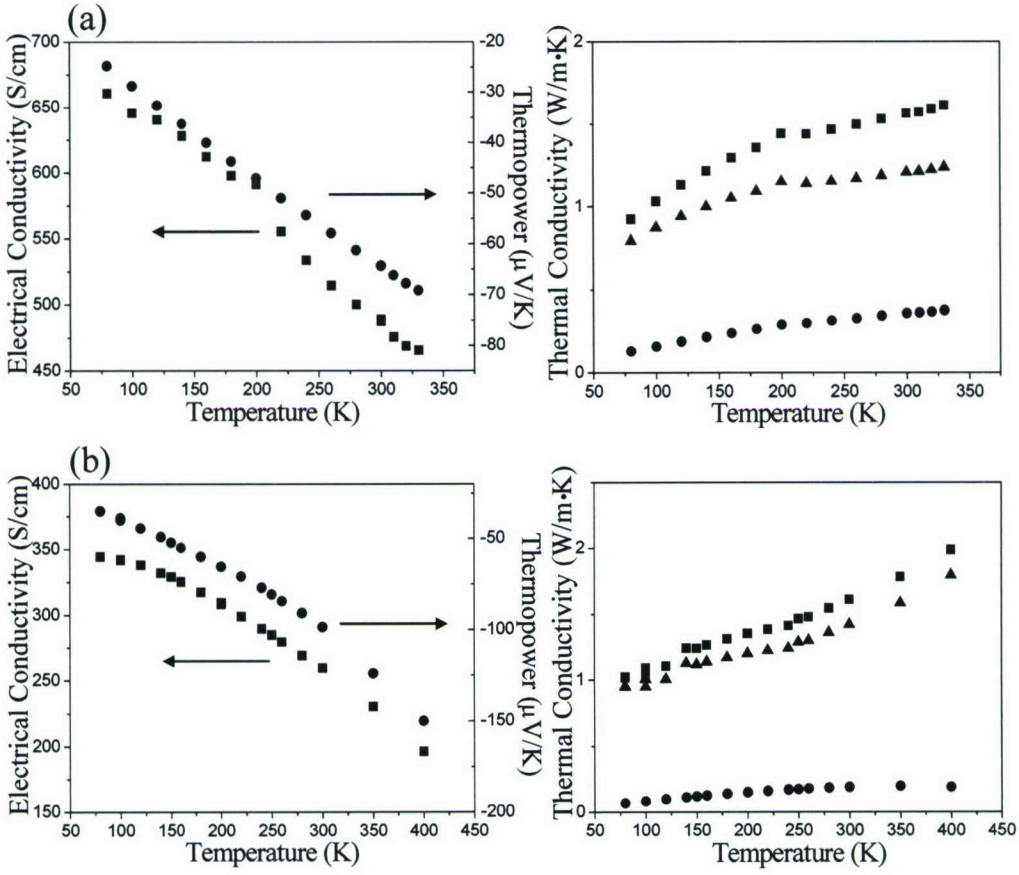

Figure 11. Variable temperature thermopower, electrical conductivity and thermal conductivity for (a) $AgBi_3S_5$ and (b) $AgSb_{0.3}Bi_{2.7}S_5$. (■ = κ_{tot}, ● = κ_e, ▲ = κ_{latt}).

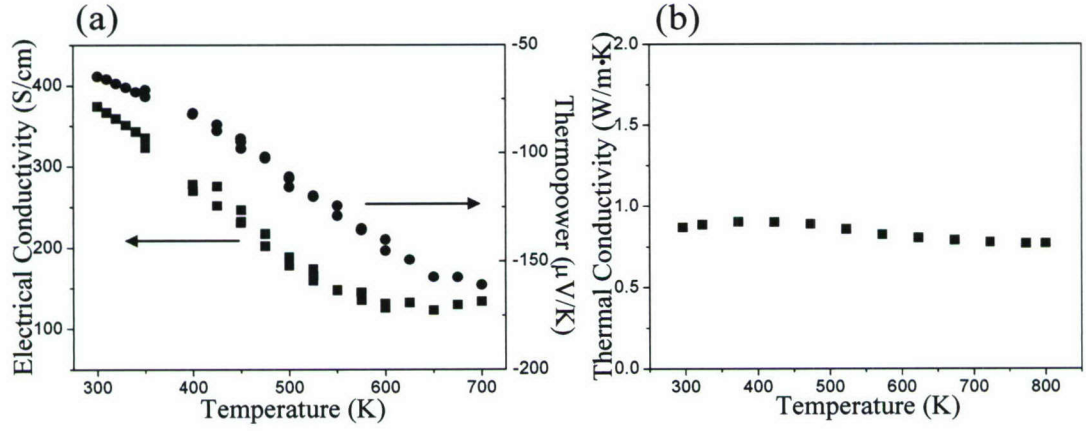

Figure 12. (a) Variable temperature thermopower and electrical conductivity data for $AgBi_3S_5$. (b) Thermal conductivity for $AgSb_{0.3}Bi_{2.7}S_5$ measured with the thermal diffusivity technique at high temperature.

Phase 2: Designing of Bulk Nano-structures with Enhanced Thermoelectric Properties

In collaboration with Dr Chris B. Murray (IBM)

The programmed assembly of quantum dot components into well-organized, densely-packed arrays represents a novel approach toward materials design. The goal of this project was to utilize quantum dot building blocks of desired thermal, electronic, and optical properties to rationally design composite materials with improved power generation, thermoelectric, and photovoltaic characteristics.

Nanocrystalline Thermoelectrically Relevant $AgPb_mSbTe_{m+2}$ Materials

Materials with compositions $AgSbTe_2$ and $AgPb_mSbTe_{m+2}$ have been shown to have promising thermoelectric (TE) properties. Recently, we described the chalcogenide compounds, $AgPb_mSbTe_{m+2}$, or LAST-m materials (LAST for Lead Antimony Silver Tellurium), several members of which can exhibit large ZT values from ~1.2 to ~1.7 (LAST-10 and -18) at 700 K.[1] High resolution transmission electron microscopy images (HRTEM) of these samples revealed endotaxially dispersed nanocrystals (i.e. regions 2 to 5 nm in size that are $AgPb_mSbTe_{m+2}$ where m~1-4.[2] The nanocrystals are reminiscent of those found in the molecular beam epitaxy-grown, high performance TE PbTe/PbSe thin films which also exhibit high ZT values (2.5 at 500 K).[3] The nanocrystals are believed to impact the thermoelectric properties at least in part by causing enhanced phonon scattering leading to very low thermal conductivity. This is amply supported by theoretical investigations which also suggest enhancements in power factor.[4] It would therefore be interesting to develop an approach of fabricating nano-phased LAST materials using bench-top inexpensive routes to conduct further studies and to investigate the link to enhanced TE performance. Here we report the synthesis of nanoparticles with compositions $AgSbTe_2$, $AgPbSbTe_3$ and $AgPb_2SbTe_4$ using reverse micellar synthesis coupled with a sodium borohydride reduction. In this route all metal ions, Ag^+, Pb^{2+}, Sb^{3+} including Te^{4+} (in Na_2TeO_3) are probably simultaneously reduced to the elemental nanoparticles which combine to form the quaternary phases.

Nanoparticles of binary chalcogenides (e.g. CdSe, PbTe) are very well studied and relatively easy to synthesize with high degree of control using a high boiling solvent such as trioctyl-phosphine oxide (TOPO) with elemental chalcogenide and a appropriate metal salt as a precursor. However, ternary or quaternary systems tend to be more challenging as they can face problems of phase separation and limitations of solubility of one or more of the precursors in a common solvent. We explored a variety of approaches including high boiling TOPO, reverse micelles and capping agents in water. The use of TOPO as a capping agent with elemental Te for the synthesis of $AgSbTe_2$ as a precursor resulted in compounds with low crystallinity and a mixture of Sb_2Te_3, Ag_2Te and Te. Another problem was the parasitic reduction of silver salts at higher temperatures yielding metallic silver precipitates in the reaction mixture. The TOPO approach suffered from a lack of proper precursors of Sb^{3+} ions with suitable solubility and was not pursued. We were successful with the capping agent and reverse micellar[5] approaches. The use of hexadecyl-amine as a capping agent yielded good quality nanoparticles with high degree and crystallinity using $NaBH_4$ reduction but often resulted in excessive aggregation. Though the fundamental particle size was fairly small, 5-15 nm, the $AgSbTe_2$ particles tended to agglomerate and form discontinuous networks. Nanoparticles exhibiting no aggregation were obtained only with a reverse

---

1 Hsu, K. F.; Loo, S.; Guo, F.; Chen, W.; Dyck, J. S.; Uher, C.; Hogan, T.; Polychroniadis, E. K.; Kanatzidis, M. G. *Science* **2004**, *303*, 818-821.

2 Quarez E., Hsu K.-F., Pcionek R., Frangis N., Polychroniadis E. K., Kanatzidis M. G. *J. .Am. Chem. Soc.* **2005**, *127*, 9177-9190.

3 Harman, T. C.; Taylor, P. J.; Walsh, M. P.; LaForge, B. E. *Science* **2002**, *297*, 2229-2232.

4 Khitun A., Wang K. L., Chen G. *Nanotechnology* **2002**, 11, 327-331.

5 Lee, Y.; Lee, J.; Bae, C. J.; Park, J.-G.; Noh, H.-J.; Park, J.-H.; Hyeon, T. *Adv. Func. Mater.* **2005**, *15*, 503-509.

micelle based approach and a borohydride based co-reduction and this method was adopted for further work.

Namely nanocrystals of $AgPb_mSbTe_{m+2}$ (m=0-2) were synthesized in a reversed micellar solution of sodium dodecyl sulfate (SDS) under ambient conditions. SDS reverse micelles were prepared using octane, 1-butanol and water as solvents. The preferred precursors were lead nitrate, potassium antimony tartrate and silver nitrate. Potassium telluride (K_2Te) or sodium tellurite (Na_2TeO_3) were used as the tellurium sources. Nanocrystals of $AgSbTe_2$ required K_2Te as the precursor whereas $AgPbSbTe_3$ and $AgPb_2SbTe_4$ were prepared with Na_2TeO_3 followed by reduction with $NaBH_4$.

The nanoparticles obtained from the synthesis had approximate spherical geometry and were crystalline with size dispersity ranging between 3 and 15 nm. The powder XRD patterns show broadening of Bragg peaks with a characteristic cubic NaCl-type structure and *Fm-3m* space group, Figure 1. The lattice parameters lie between those of $AgSbTe_2$ and PbTe and vary systematically with *m* (see Table 1) which is evidence for the successful incorporation of $AgSbTe_2$ into the PbTe lattice. They also compare well to those of the bulk LAST materials synthesized with conventional solid state synthesis. The average particle sizes estimated from line broadening analysis are in the range of ~4.5-5.2 nm and in agreement with the TEM observations, see Table 1.

The nanoparticles (*m*=0-2) show well defined energy band-gaps in the range of ~0.6-0.7 eV, Figure 1B and Table 1. These band-gaps are significantly wider than the corresponding values of the bulk materials of ~0.3 eV which is consistent with the expected size dependent blue shift due to quantization of the energy levels in the nanocrystals.

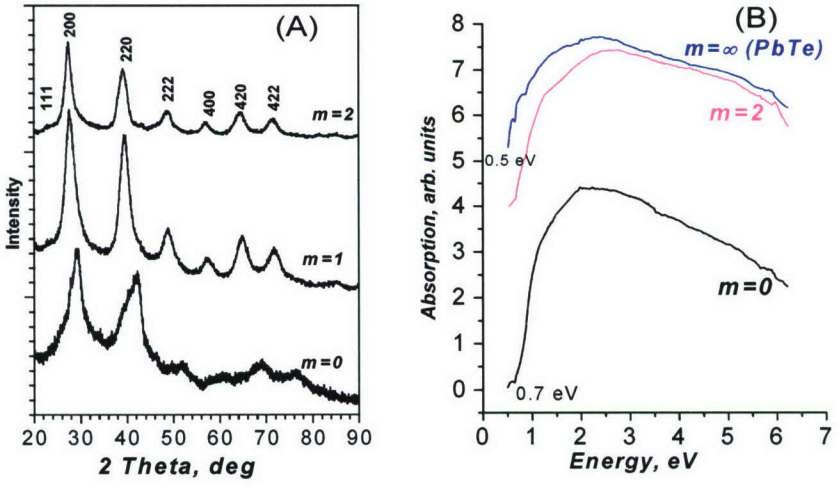

Figure 1: (A) XRD patterns (Cu K_α rad) of nanoparticles of $AgSbTe_2$ (*m*=0), $AgPbSbTe_3$ (*m*=1) and $AgPb_2SbTe_4$ (*m*=2). (B) Solid state optical band gap measurement for *m*=0, 2 and for comparison PbTe (*m*=∞). Diffuse reflectance data converted to absorption using the Kubleka-Munk function (SI section). The spectra are offset along the y-axis.

Table 1: Elemental composition, lattice constant (Å), average particle size and energy band gap (E_g) for $AgPb_mSbTe_{m+2}$ nanoparticles.

Sample	Composition (esd ±4-5%)[1]	Cell parameter, (Å)	Particle size[2] (nm)	E_g, (eV)[3]
m=0	$Ag_{1.07}SbTe_{2.08}$	6.10(1)	4.3	0.7(1)
m=1	$Ag_{0.95}PbSb_{1.07}Te_{2.67}$	6.42(1)	4.6	0.6(1)
m=2	$Ag_{1.15}Pb_2Sb_{0.86}Te_{4.10}$	6.45(1)	5.2	0.6(1)
m=∞	$Pb_{1.00}Te_{0.99}$	6.55(1)	5.0	0.5(1)

1) SEM-EDS analysis. 2) Average size from XRD data (error ±10%). 3) The optical spectra were measured in the diffuse reflectance mode on a Shimadzu UV-Vis-NIR spectrophotometer (UV3101 PC).

Figure 2A shows a low magnification TEM image of $AgSbTe_2$ indicating nanoparticles ranging from 3-15 nm, over a large area. Similar particle size distributions were obtained for $AgPb_2SbTe_4$ and

$AgSbPbTe_3$, Figure 2B,C. Figure 2D shows a HRTEM image of a single nanocrystal of $AgPb_2SbTe_4$ prepared with the reverse micellar approach. Energy dispersive X-ray spectroscopy analysis (EDS) on individual nanoparticles indicated the presence of all four elements. The lattice fringes are clearly visible in the image indicating high atomic order. We did not observe any evidence for amorphous products by TEM. Furthermore, the XRD patterns as well as SEM investigations indicated no evidence for adventitious phases such as Ag, Ag_2Te, Sb_2Te_3 or Te (detection limit ~±5%). Electron diffraction patterns obtained from collections of these nanoparticles indicated only rock-salt *Fm*-3*m* structure type, Fig. 2C(inset). EDS analysis of $AgPb_mSbTe_{m+2}$ in a scanning electron microscope showed presence of Ag, Sb and Pb and Te in atomic ratios summarized in Table 1.

In conclusion, a facile synthesis of nanoparticles of the thermoelectrically relevant $AgPb_mSbTe_{m+2}$ was accomplished for the first time in reverse micelles. The procedure offers several distinct advantages for the synthesis of crystalline nanoparticles of thermoelectric ternary and quaternary lead chalcogenides. The process is convenient, general and extendable to nanoparticles with higher *m* values including m=∞ (i.e. PbTe). It is also low cost and environmentally friendly, by employing common water soluble metal salts. As a result, the synthesis could be scaled to a multi-gram level in a single reaction. We are currently investigating methods to process these nanomaterials into compact shapes and measure their thermoelectric properties.

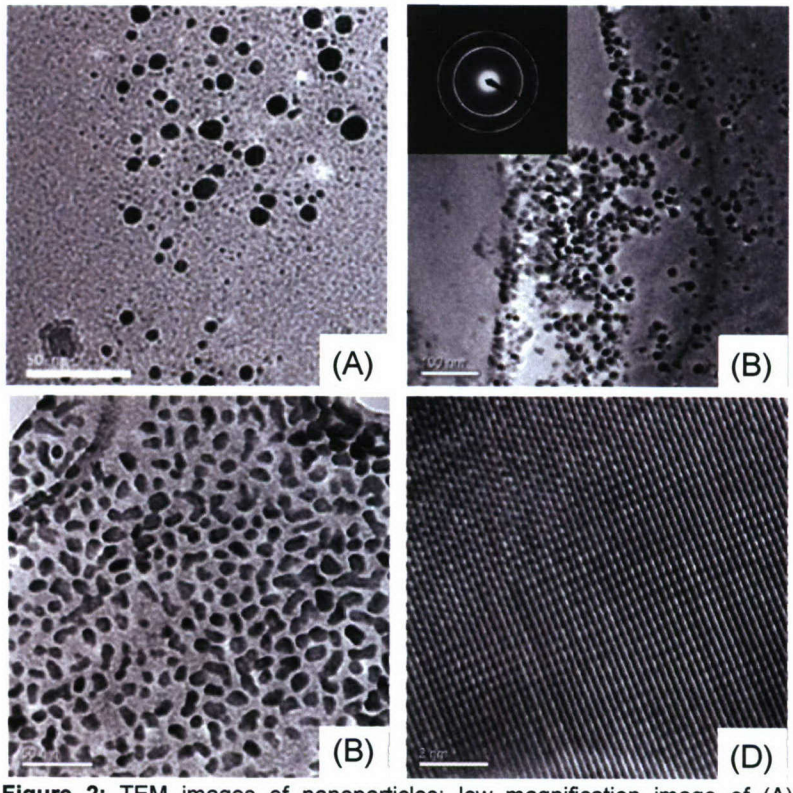

Figure 2: TEM images of nanoparticles: low magnification image of (A) $AgSbTe_2$, (B) $AgPbSbTe_3$ and (C) $AgPb_2SbTe_4$. Inset: electron diffraction pattern of a collection of nanoparticles consistent with *Fm*-3*m* lattice. (D) HRTEM image of $AgPb_2SbTe_4$ showing the presence of lattice fringes with ~6.5 Å period. The scale bars in the four images are 50nm, 50 nm, 100 nm and 2 nm respectively. EDS analysis on individual nanocrystals indicated the presence of all four elements. High resolution TEM images were obtained with 200 kV JEOL JEM 2200FS microscope.

Additionally, nanoparticles of LAST could show unusual electronic and optical properties that could help understand the corresponding bulk materials. This is a challenging task owing to a coating of the organic layer surrounding the nanoparticles. Various techniques including annealing, extraction of surfactants with suitable solvents, followed by cold or hot pressing, for conductivity and thermopower measurements are in progress.

Research accomplishments

1. **Ag_2Te Nanocrystal Synthesis** An original synthesis of Ag_2Te nanocrystals has been developed. This represents the first controlled method to produce nanocrystals of this candidate thermoelectric material. Both the size and the shape of the nanocrystals produced may be controlled. These samples have been characterized via TEM, XRD, and absorbance spectroscopy. A controlled route to Ag_2Te quantum dots meets a core project objective.

2. **Synthesis of Multicomponent Nanocrystal Assemblies** Superlattice assemblies containing both PbTe (covered in the prior report) and Ag_2Te have been prepared and structurally characterized by TEM, SAXS, and XRD. Access to these multicomponent solids was one of the core project objectives.

3. **Fabrication and Measurement of Nanocrystal Transistors** The electronic properties of single-component thin-film nanocrystal solids of PbTe and Ag_2Te nanocrystals has been carried out. This represents some of the earliest successful reports of high-performance nanocrystal transistors. Integration of these materials into functional electronic devices is critical to fully characterizing their carrier transport properties.

4. **Electronic Characterization of Multicomponent Solids** The multicomponent PbTe/Ag_2Te solids described above were also integrated into electronic devices and studied. These studies uncovered dramatically enhanced (~100 fold in 1:1 mixtures) electronic conductance in these composite systems. This introduces a new concept of using nanoparticles as dopants in structured assemblies, a potentially novel way to enhance the electronic conductance of thermoelectric solids. Electronic characterization of these multicomponent solids meets a core project objective.

5. **Thermal Characterization of Nanocrystal Solids** An effective collaboration was established between Professor David Cahill's group (another ONR project member) and our group. We have performed time-domain thermoreflectance (TDTR) measurements on the PbTe, Ag_2Te, and multicomponent (PbTe/Ag_2Te) thin-film nanocrystal solids. This collaboration is ongoing, however, we can report very low thermal-conductivity values for these solids (0.6 to 0.9 W/mK). Measurement of the thermal properties of these nanocrystal solids meets a key project goal.

6. **Scale-up of Nanocrystal Syntheses** The Ag_2Te synthesis was successfully scaled-up to the ~10g range in correspondence to the PbTe synthesis. Scale-up of product synthesis meets a central project objective.

Non-aqueous methods to synthesize quantum dots of both lead selenide (PbSe) and lead telluride (PbTe) have been developed and refined, Figure 3. Both the size and the shape of the nanocrystals produced may be controlled. These samples have been characterized via TEM, XRD, and absorbance spectroscopy. The lead chalcogenide nanocrystal syntheses have been scaled up to produce ~10g (~27mmol) of PbSe quantum dots for a 3 minute reaction time.
The electronic properties of these PbSe films have been measured under three different sets of conditions: as-deposited, after heat treatment, and after chemical dopin, Figure 4g. Chemical doping methods have been developed which enable good n-type and p-type films of these nanocrystals to be controllably produced.

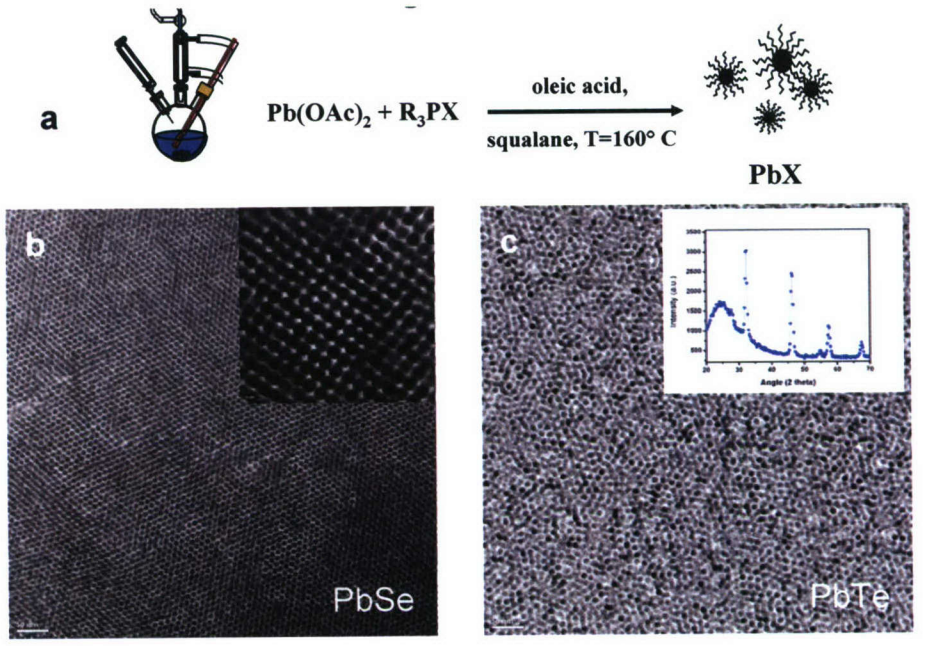

Figure 3. a.) Schematic depicting the experimental procedure used to synthesize lead chalcogenide nanocrystals. A lead salt is solubilized by oleic acid in squalane and heated up to high temperature at which point a phosphine-chalcogen complex is injected. The reaction is allowed to proceed for a few minutes, and then the product is recovered and washed to yield a black solid consisting of lead chalcogenide quantum dots. b.) Transmission electron micrograph (TEM) of ~8nm PbSe quantum dots. The inset shows a magnified image of these nanocrystals. c.) TEM image of ~6nm PbTe quantum dots. The inset shows a X-ray diffraction pattern collected off a 10nm sample of PbTe nanocrystals.

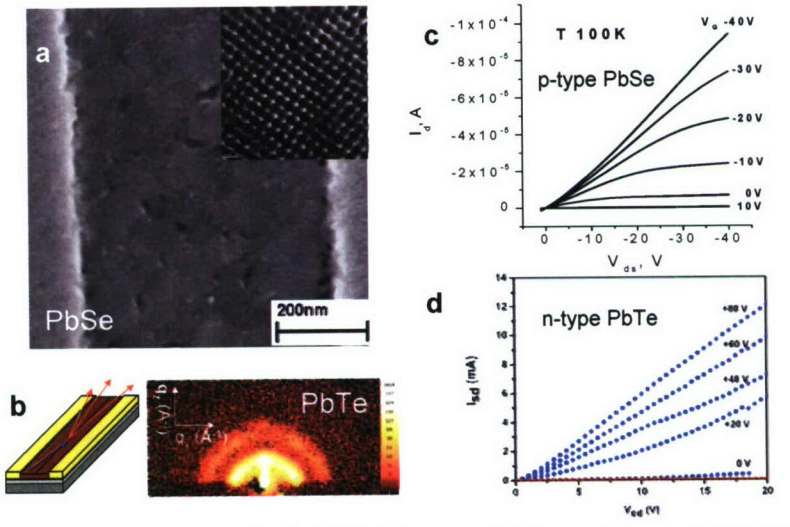

Figure 4. a.) Scanning electron micrograph of a PbSe film assembled on a silicon substrate in the channel between two gold electrodes. This is the experimental setup used to characterize the electronic transport of these films described in this overview. The inset shows a magnified portion of this nanocrystal film, demonstrating its excellent uniformity and ordering. b.) A cartoon depicting the experimental geometry used for the grazing incidence small-angle X-ray scattering (GISAXS) experiments. As described above, the PbX film is self-assembled on a silicon substrate inbetween two gold electrodes. The rings in the GISAXS pattern demonstrate the excellent ordering of this film in all three dimensions. c.) Electronic characterization of a p-type PbSe transistor. Here the drain current was measured as the source-drain voltage was swept at a fixed value of the gate voltage. These measurements were

carried out in 10V increments of the gate voltage, as shown. d.) Electronic characterization of an n-type PbTe transistor using the same approach and experimental geometry outlined above.

A novel non-aqueous route to synthesize germanium telluride (GeTe) has been developed, Figure 5. This represents an entirely new method toward production of this material, and furthermore one that is carried out at moderate temperatures and ambient pressure. This material has also been fully characterized as above. The synthesis of bulk GeTe has been modified to consistently generate nanocrystalline GeTe. This is the first known report of the synthesis of nanocrystalline GeTe. These materials have also been fully characterized as described above.

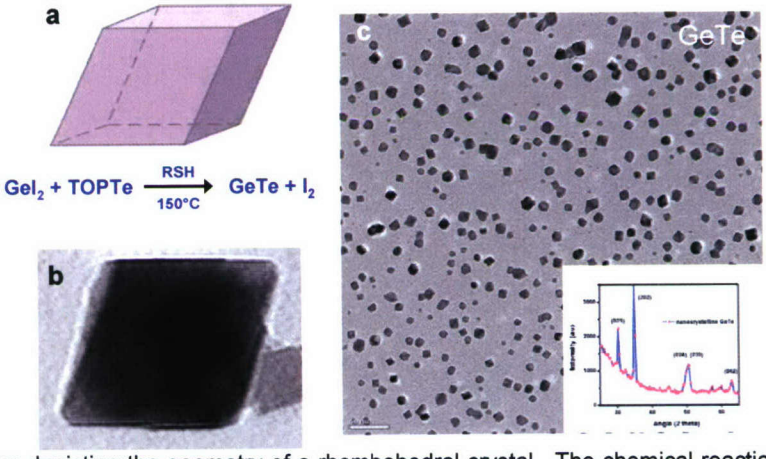

Figure 5. a.) Cartoon depicting the geometry of a rhombohedral crystal. The chemical reaction used to synthesize the GeTe rhombohedra (and bulk solids) is outlined below the rhombohedron. b.) High-resolution TEM image of a GeTe rhombohedron whose sides measure 20nm in length. Here the distortion from the cubic geometry is clearly visible. c.) Low-resolution TEM image of GeTe rhombohedra isolated from the synthetic procedure described in the text. Close inspection shows that it is common for several rhombohedra to undergo oriented attachment and link with one another. The inset shows a X-ray diffractogram recorded on a GeTe nanocrystalline sample. The broadening of the X-ray diffraction peaks inherent to nanoscale materials obscures the splitting of the (024) and (220) peaks, which we observe in our analysis of bulk GeTe.

Unmet Objectives

1. To create continuous solid aggregates (made from nanocrystals prepared in this project) with high electrical conductivity.
2. To prepare n-type and p-type heavily doped nanocrystals.
3. To further refine the synthetic procedure for GeTe nanocrystals. The properties of the PbTe/Ag_2Te assemblies were very fruitful, so the GeTe nanocrystals ultimately received less attention.

4. The development of methods enabling (and the characterization of) the Seebeck coefficients for these new classes of materials.

5. The production of a large-scale (~cm size) pellet of the multicomponent solids for complete characterization.

Relevant Publications generated during this project (2002-2006)

1) "Improvement in the Thermoelectric Properties of Pressure-tuned β-$K_2Bi_8Se_{13}$" J. F. Meng, N. V. Chandra Shekar, M. Kanatzidis, and J. V. Badding, *J. Applied Physics*, **2003**, 94, 4485-4488.

2) "Tropochemical Cell-Twinning in the Quaternary Bismuth Selenides $K_xSn_{6-2x}Bi_{2+x}Se_9$ and $KSn_5Bi_5Se_{13}$" A. Mrotzek and M. G. Kanatzidis, *Inorg Chem* **2003**, 42

3) "Thermoelectric Properties and Site Selective Rb^+/K^+ Distribution in the $K_{2-x}Rb_xBi_8Se_{13}$ Series" T. Kyratsi, D.-Y. Chung, J. R. Ireland, C. R. Kannewurf and M. G. Kanatzidis, *Chem. Mater.*, **2003**; 15; 3035-3040.

4) "Synthesis, crystallographic studies, and characterization of $K_2Bi_8Se_{13-x}S_x$ solid solutions" Kyratsi T, Kanatzidis MG *Z anorg allg Chem* **2003**, 629, 2222-2228.

5) "Surface effects in layered semiconductors Bi_2Se_3 and Bi_2Te_3" Urazhdin S, Bilc D, Mahanti SD, Tessmer SH, Kyratsi T, Kanatzidis MG *Phys. Rev. B* **2004**, 69, 85313

6) . Synthesis, crystal structure and thermoelectric properties of β-$K_2Bi_8Se_{13}$ solid solutions. Kyratsi, Theodora; Chung, Duck Young; Dyck, Jeff S.; Uher, Ctirad; Lal, Sangeeta; Loo, Sim; Hogan, Tim; Ireland, John; Kannewurf, Carl R.; Hatzikraniotis, Evripides; Paraskevopoulos, Konstantinos M.; M. G. Kanatzidis, *Materials Research Society Symposium Proceedings* (2004), 793 (Thermoelectric Materials 2003--Research and Applications), 359-364.

7) Synthesis and thermoelectric properties of $AgBi_3S_5$. Kim, Jun-Ho; Bilc, Daniel; Loo, Sim; Short, Jarrod; Mahanti, S. D.; Hogan, Tim; Kanatzidis, Mercouri G.. *Materials Research Society Symposium Proceedings* (2004), 793(Thermoelectric Materials 2003--Research and Applications), 201-206.

8) Effect of K/Bi ordering on the electronic structure of $K_2Bi_8Se_{13}$. Bilc, Daniel I.; Larson, Paul; Mahanti, S. D.; Kanatzidis, M. G.. *Materials Research Society Symposium Proceedings* (2004), 793(Thermoelectric Materials 2003--Research and Applications), 161-166.

9) "A New Thermoelectric Material : $CsBi_4Te_6$" Duck-Young Chung, Tim P. Hogan, Melissa Rocci-Lane, Paul Brazis, John R. Ireland, Carl R. Kannewurf, Marina Bastea, Ctirad Uher, and Mercouri G. Kanatzidis, *J. Am. Chem. Soc.* **2004**, *126*(20); 6414-6428.

10). "Thermoelectric Properties of β-$K_2Bi_{8-x}Sb_xSe_{13}$ Solid Solutions a Promising Series for High Temperature Applications". Th. Klratsi, D-Y.Chung, J.S. Dyck, C. Uher, E. Hatzikraniotis, K.M. Paraskevopoulos and M.G. Kanatzidis, Proceedings of 2nd European Conference on Thermoelectrics of the European Thermoelectric Society Poland, Kraków, September 15-17, 2004.

11). Lattice thermal conductivity of $K_2(Bi_{1-z}Sb_z)_8Se_{13}$ solid solutions Kyratsi T, Hatzikraniotis E, Paraskevopoulos K. M, Dyck JS, Shin HK, Uher C, Kanatzidis MG *J. Appl. Phys.* **2004**, 95, 4140-4146.

12). "Structural Evolution and Phase Homologies for "Design" and Prediction of Solid-State Compounds" Kanatzidis, M. G. *Acc. Chem. Res.* **2005**, 38, 359-368.

13). Bilc, D. I.; Mahanti, S. D.; Kyratsi, T.; Kanatzidis, M. G.; Larson, P. "Electronic structure of $K_2Bi_8Se_{13}$" *Phys. Rev. B* **2005**, 71 (8): Art. No. 085116.

14). Design in solid state chemistry based on phase homologies. Sb_4Te_3 and Sb_8Te_9 as new members of the series $(Sb_2Te_3)_m{\cdot}(Sb_2)_n$. Pierre F. P. Poudeu and Mercouri G. Kanatzidis, *Chem. Commun.* **2005**,2672-2674.

15). "Crystal Growth, Thermoelectric Properties and Electronic Structure of $AgBi_3S_5$ and $AgSb_xBi_{3-x}S_5$ (x=0.3)" Jun-Ho Kim, Duck-Young Chung, Daniel Bilc, Sim Loo, Jarrod Short, Subhendra. D. Mahanti, Tim Hogan and Mercouri G. Kanatzidis, *Chem. Mater.*, **2005**, 17, 3606-3614.

16) "Optical Properties of Thermoelectric Alkali Metal Chalcogenide Compounds $K_2Bi_{8-x}Sb_xSe_{13}$" E. A. Hatzikraniotis, Th. Kyratsi, T Zorba, K. M. Paraskevopoulos, M. G. Kanatzidis *Mater. Res. Soc. Symp. Proc.* **2005**, *886*, 0886-F08-01.

17) "Thermoelectric Properties of $K_2Bi_8Se_{13-x}S_x$ Solid Solutions" Theodora Kyratsi, Sangeeta Lal, Tim Hogan, Mercouri G. Kanatzidis *Mater. Res. Soc. Symp. Proc.* **2005**, *886*, 0886-F08-02.

18) "Substitutions in the Homologous Family $CsPb_mBi_3Te_{5+m}$ and Preliminary Thermoelectric Results" Aurelie Gueguen, Eric Quarez, Mercouri G. Kanatzidis *Mater. Res. Soc. Symp. Proc.* **2005**, *886*, 0886-F08-06.

19). Kim JH, Chung DY, Kanatzidis MG "A new chalcogenide homologous series $A_2[M_{5+n}Se_{9+n}]$ (A = Rb, Cs; M = Bi, Ag, Cd)", *Chem. Commun.* **2006**, (15): 1628-1630.

20). Karkamkar AJ, Kanatzidis MG Chemical routes to nanocrystalline thermoelectrically relevant $AgPb_mSbTe_{m+2}$ materials *J. Am. Chem. Soc.* **2006**, 128 (18): 6002-6003.

21) "Low thermal conductivity in thin-film nanocrystal solids measured by time-domain thermoreflectance," Jeffrey J. Urban, Catalin Chiritescu, D.C. Cahill, and C.B. Murray, *manuscript in preparation for Appl. Phys. Lett.* (2007).

22) "Synergism in binary nanocrystal superlattices leads to enhanced *p*-type conductivity in self-assembled PbTe/Ag_2Te thin films," Jeffrey J. Urban, Dmitri V. Talapin, Elena V. Shevchenko, Cherie R. Kagan, and C.B. Murray, *Nature Materials* **6(2)** 115-121 (2007). Work highlighted in Nature **445** 492-493 (2007).

23) "Chemical trends in lead chalcogenide transistors," Dmitri V. Talapin, Jeffrey J. Urban, and C.B. Murray, *manuscript in preparation for J. Am. Chem. Soc.* (2007).

24) "Self-assembly of PbTe quantum dots into nanocrystal superlattices and glassy films," Jeffrey J. Urban, Dmitri V. Talapin, Elena V. Shevchenko, and C.B. Murray, *J. Am. Chem. Soc.* **128(10)**, 3248-3255 (2006). Work highlighted in Photonics Spectra, April 2006
